Conference on Modelling Fluid Flow (CMFF'25)
The 19th International Conference on Fluid Flow Technologies
Budapest, Hungary, August 26 - August 29, 2025

THE EFFECT OF BUBBLE PARAMETERS ON THE MIXING IN A BUBBLE COLUMN WITH COUNTER-CURRENT LIQUID FLOW

Péter KOVÁTS[1], Katharina ZÄHRINGER[2]

[1,2] Laboratory of Fluid Dynamics and Technical Flows, Otto-von-Guericke-Universität Magdeburg. Universitätsplatz 2, D-39106 Magdeburg, Germany. Tel.: +49 391 - 67 58654, Fax: +49 391 - 67 52840 *E-mail: peter.kovats@ovgu.de

ABSTRACT

Bubble columns have been widely studied concentrating mostly on the bubble parameters, and gas/liquid motion. However, bubble generated mixing in the column is rarely analysed, especially with counter-current liquid flow. For this reason, experiments with Laser Induced Fluorescence (LIF) applying Sulforhodamine G as fluorescent tracer dye were performed in a laboratory-scale counter-current flow bubble column. In these experiments the efficiency of the bubble generated mixing was investigated by varying the bubble size, gas and liquid flow rates and the dye inlet position. Additionally, the mixing results were compared to the liquid flow fields obtained from Particle Image Velocimetry (PIV). From the results it is obvious, that bubble induced mixing leads to a good dye distribution inside the column, compared to a single-phase flow without bubbles. It has been found, that the larger the bubbles the higher the bubble induced vorticity, which leads to a better local and therefore global mixing. The highest counter-current liquid flow rate led to a more concentrated dye jet, which was less dispersed than at lower liquid flow rates. As a result, the combination of large bubbles generated with the 3.6 mm capillaries, and a moderate counter-current liquid flow rate (11.1 $l\cdot min^{-1}$) led to the best mixing performance in the investigated bubble column reactor.

Keywords: bubble column reactor, dispersed two-phase flow, counter-current flow, LIF, PIV, mixing

NOMENCLATURE

a	[mm]	major semi-axis
b	[mm]	minor semi-axis
c	[$mg\cdot l^{-1}$]	measured concentration
c_{min}	[$mg\cdot l^{-1}$]	minimum background concentration
c_{max}	[$mg\cdot l^{-1}$]	injected dye concentration
c_n	[$mg\cdot l^{-1}$]	normalized concentration
$c_{n,exp}$	[$mg\cdot l^{-1}$]	experimental normalized concentration
$c_{n,theor}$	[$mg\cdot l^{-1}$]	theoretical normalized concentration
c_{norm}	[$mg\cdot l^{-1}$]	normalized dye concentration ratio, $c_{n,exp}/c_{n,theor}$
d	[m]	column diameter
ESD	[mm]	equivalent sphere diameter
h	[m]	column height
j	[$m\cdot s^{-1}$]	superficial velocity
Q	[$l\cdot h^{-1}$]	volume flow rate
v_b	[$m\cdot s^{-1}$]	bubble velocity
Re_c	[-]	column Reynolds number

Subscripts and Superscripts

g	gas
l	liquid

1. INTRODUCTION

A well-known example of a multiphase flow is gas bubbles in a liquid phase, which occurs in a great variety of natural phenomena, in chemical or biological processes, in waste water treatment, in nuclear engineering or even in everyday life, like in soft drinks. Bubbles are often used for mixing, since they provide favourable mixing and mass transfer properties combined with gentle agitation and low shear stressing of the mixed fluids, compared to other stirring tools. Mixing of liquids is a very energy intensive operation depending on among others the duration of the mixing, the liquid viscosity and reactor geometry. The optimal mixing process would ensure for a minimal power consumption but maximal homogeneity of the mixture. Mixing, induced by the rising bubbles in a bubble column and the resulting interaction between chemical reaction and hydrodynamics in the column is a challenging research field due to its complexity. Traditionally, the mixing time and mixing efficiency is measured in stirred vessels or in bubble columns in an invasive manner with pH

Copyright© Department of Fluid Mechanics, Budapest University of Technology and Economics and the Authors

or conductivity probes [1-4]. These measurement techniques are robust, but the probes disturb the flow and the measurement is only point-wise.

For a global mixing characterization different methods are available. One of them is based on acid-base reaction and the colour change of a dye pH-indicator. This method is inexpensive and simple, but it integrates the colour of the whole depth of the investigated volume, which means an averaged mixing characterization in the depth. Therefore, it is efficient for a rough estimation, but ineffective for detailed investigations [2, 5, 6]. Electrical resistance tomography (ERT), which can provide mixing information also in opaque liquids, is also an integrating measurement technique. However, the spatial resolution of these methods are far from common imaging and the correct data reconstruction is very difficult [5, 7, 8]. Besides these techniques, the dye distribution, concentration and mixing homogeneity can be obtained with high temporal and spatial resolution in a 2D plane with planar LIF [5, 9-12]. Because of its accuracy and resolution, this technique was selected for the experiments presented in this paper.

Unfortunately, experimental investigations of bubble-induced mixing and its influence on mass transfer or mixing characterisation and visualisation in bubble columns are rarely found in the literature.

A research group at the IMFT in Toulouse analysed mixing and concentration fluctuations in bubble swarms [13, 14] and investigated mixing in a pseudo-2D bubble column [15]. Also, a group at HZDR in Dresden worked on bubble-induced turbulence and bubble swarms extensively [16-19].

Studies of the mixing behaviour of bubble columns [20-23] or for bubble-induced turbulence [24-28] using simulations can also be found sporadically in the literature.

Unfortunately, experimental studies relating mixing and bubble-induced turbulence in the same bubble column cannot be found.

For this reason, in the present study, an experimental measurement campaign has been performed to obtain the necessary data for a further understanding of mixing processes in bubbly flows with bubble-induced turbulence. Different gas inlet configurations are used to investigate the influence of bubble size and gas and liquid flow rates on mixing in the counter-current model bubble column.

2. EXPERIMENTAL SET-UP

To characterise the liquid flow and mixing in the bubble column, three optical measurement methods have been applied. First, for the liquid phase, Particle Image Velocimetry (PIV) was used to examine the hydrodynamics of the two-phase flow. Then, combined Laser-Induced Fluorescence (LIF) and shadow imaging measurements have been executed in the square laboratory-scale counter-current bubble column, which is made of acrylic glass with an inner side length of d= 0.100 m and a height of h= 2 m (Figure 1, #1). In both experiments, the bubbles were generated with 7 capillaries placed in line in the centre of the bubble column and 500 mm above its bottom (Figure 1, #2). Capillaries with three different sizes, produced air bubbles in a size range of 1 to 9 mm. The bubble column and its peripheral devices have been described in detail in previous papers [29, 30]. The investigated experimental cases are listed in Table 1.

Table 1. Experimental conditions.

Capillary inner diameter/ material	j_g [m· s^{-1}]	Q_g [l· h^{-1}]	j_l [m· s^{-1}]	Q_l (Counter-current) [l· min^{-1}]	Re_c (Column Reynolds number)
0.13 mm/ stainless steel	2.8· 10^{-4}	10	0	0	0
			1· 10^{-3}	0.6	100
			5.2· 10^{-3}	3.1	500
			1.9· 10^{-2}	11.1	1800
			9.3· 10^{-2}	55.5	9000
0.18 mm/ Teflon	2.8· 10^{-4}	10	0	0	0
			1· 10^{-3}	0.6	100
			5.2· 10^{-3}	3.1	500
			1.9· 10^{-2}	11.1	1800
			9.3· 10^{-2}	55.5	9000
3.6 mm/ PEEK	2.7· 10^{-4}	9.7	0	0	0
	1.3· 10^{-3}	48.4	1· 10^{-3}	0.6	100
			5.2· 10^{-3}	3.1	500
			1.9· 10^{-2}	11.1	1800
			9.3· 10^{-2}	55.5	9000

The images have been recorded over the entire measurement section (1 m) of the column with four 5 Mpixel cameras (LaVision Imager sCMOS, Figure 1, #3) equipped with 50 mm Nikon Micro lenses and appropriate filters to record the emitted light of the injected fluorescent dye Sulforhodamine G or the fluorescence signal of the Rhodamine B doped polymethyl methacrylate (PMMA) PIV seeding particles (mean diameter: 1-20 µm). The cameras were focused on the laser light sheet generated by a Nd:YAG double pulse laser (Evergreen PIV, 532 nm) in the centre plane of the column, in line with the bubble injection device. For the LIF experiments, the fluorescent dye was injected into the column with a syringe at 500 mm in the centre plane of the column through a stainless steel capillary with a concentration of c_{max} = 0.1 mg· l^{-1} and 10 ml· min^{-1} flow rate. Simultaneously to the LIF images, shadow images of the bubbles were also recorded, to be able to mask the bubble shapes from the LIF images during image processing and to obtain simultaneously the bubble size distribution of the specific measurement condition. To this end, eight high-power LEDs were used together with a sheet of thin drawing paper, as light diffuser, on the back wall of the column to obtain homogeneous light distribution for the shadow images of the bubbles. The bubble shadow images were acquired on the second frame of the cameras and triggered with an inter-frame time of 40 µs to the LIF images,

Copyright© Department of Fluid Mechanics, Budapest University of Technology and Economics and the Authors

which assured that bubbles did not move noticeably in-between both frames.

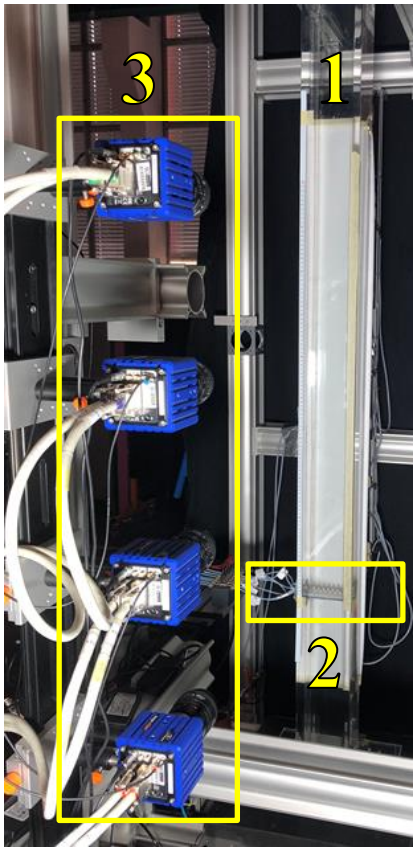

Figure 1. Experimental setup: bubble column (1), gas distributor (2), cameras (3).

The images were calibrated with a 3D calibration target over the whole measurement section for all measurement methods. During the experiments, 3x1500 LIF/Shadow images and overall 4000 PIV images were recorded with 5 Hz recording rate for each investigated case.

3. DATA PROCESSING

All recorded images were processed in DaVis 8.4 (LaVision). In the case of PIV, flow fields were calculated from the recorded double-frame images with a cross-correlation algorithm (multi-pass) with a decreasing interrogation window size from 64x64 pixels to 32x32 pixels, with 50% overlap. To remove false vectors and refine the vector fields, especially in the vicinity and shadows of the bubbles, a median filter was applied. After combining the results of all four measurement windows (obtained simultaneously with the four cameras), a full view of the liquid flow field within the column has been obtained. From these vector fields mean velocity fields were calculated for each investigated case. Moreover, probability density functions were generated to investigate the distributions of the horizontal and vertical velocity components as well as the distribution of the vorticity.

In the case of the LIF images for the mixing analysis, the bubbles were masked with the help of the recorded bubble shadow images (Figure 2). In the next step, the recorded fluorescent light intensities were converted into Sulforhodamine G concentrations with the help of a linear calibration curve, determined before.

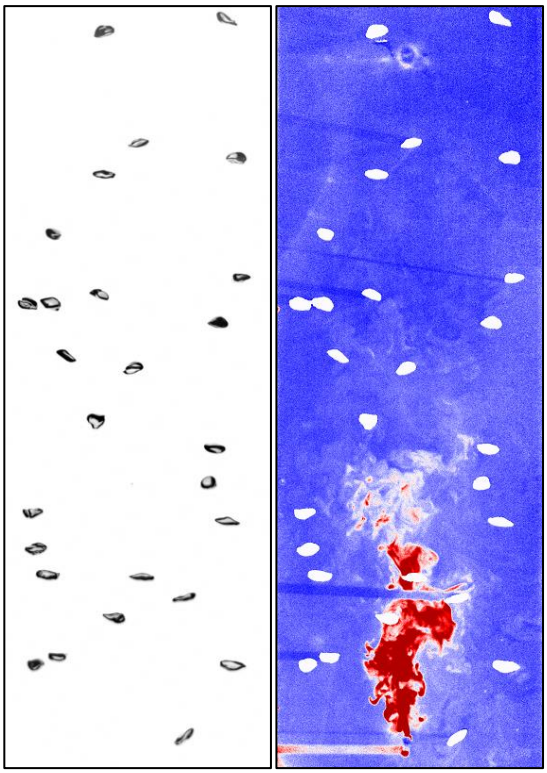

Figure 2. Image processing: shadow image with subtracted background (left), binarised mask from shadow image applied to the LIF image (right).

For the quantification of mixing, a mixing coefficient has been defined:

$$c_n = \frac{c - c_{min}}{c_{max} - c_{min}} \qquad (1)$$

where c_{max} is the injected dye concentration and c_{min} corresponds to a minimum background intensity, which is zero in theory, while for the experiments it is equal to the equivalent intensity of the first recorded image for each run, when no dye is in the system, and therefore it is close to zero. To be able to compare the results from different counter-current liquid flow rates, the experimental normalised concentrations $c_{n,exp}$ have been divided by the normalised theoretical concentration for perfect mixing $c_{n,theor}$ of the respective counter-current liquid flow rate. In the case of perfect

Copyright© Department of Fluid Mechanics, Budapest University of Technology and Economics and the Authors

mixing, one obtains $c_{norm} = 1$, in the other cases, c_{norm} is calculated as:

$$c_{norm} = \frac{c_{n,exp}}{c_{n,theor}} \quad (2)$$

To compare the mixing efficiency for different investigated cases the normalised dye concentration ratios at 300 s after injection start will be used in the discussion of the results.

The quantification of the mixing intensity has been described more in detail in a separate paper [29].

4. DISCUSSION

The bubble parameters measured in the bubble column at different flow conditions, and for the flow parameters relevant in the current paper, are listed in Table 2 [30, 31].

Table 2. Global mean results of bubble diameters and velocities.

Capillary diameter [mm]	Q_g [l· h^{-1}]	Q_l [l· min^{-1}]	*ESD* [mm]	v_b [m· s^{-1}]	Aspect ratio
0.13	10	stagnant	2.71	0.31	0.63
0.13	10	0.6	2.7	0.31	0.62
0.13	10	3.1	2.7	0.31	0.62
0.13	10	11.1	2.72	0.30	0.63
0.13	10	55.5	2.91	0.22	0.64
0.18	10	stagnant	3.67	0.30	0.54
0.18	10	0.6	3.47	0.30	0.55
0.18	10	3.1	3.55	0.30	0.55
0.18	10	11.1	3.59	0.28	0.55
0.18	10	55.5	3.75	0.21	0.55
3.6	10	stagnant	6.01	0.28	0.5
3.6	10	0.6	6.03	0.28	0.5
3.6	10	3.1	6.85	0.32	0.53
3.6	10	11.1	6.04	0.27	0.51
3.6	10	55.5	5.9	0.20	0.53
3.6	50	stagnant	6.85	0.32	0.53
3.6	50	0.6	6.89	0.32	0.52
3.6	50	3.1	6.86	0.32	0.53
3.6	50	11.1	6.88	0.30	0.53
3.6	50	55.5	6.6	0.24	0.57

The results show that with increasing gas volume flow rate, the bubble size increases, as well as with an increasing capillary size. The bubble size also increases with increasing counter-current liquid flow rate, except at the largest capillary, where no clear trend can be found. In contrast, the bubble velocity is generally decreasing with an increasing bubble size, and it evidently decreases with an increasing counter-current liquid flow. Also, a slight growth can be found in bubble velocities with increasing gas flow rate. Interestingly, the bubble aspect ratio (*b*/*a*) remains generally the same for one capillary size, independent of the counter-current liquid or gas flow rate, but it decreases with increasing capillary and therefore bubble size. It also has to be mentioned that the shape of the large bubbles generated with the largest capillary is more unstable, than that of the smaller ones. This form-instability is also reflected in the global mean results, mostly in the changing aspect ratios.

All these global parameters (bubble size, velocity, and aspect ratio) have strong influences on mixing in the bubble column. These impacts will be discussed hereafter.

4.1. Mixing results

Figure 3 shows exemplary snapshots of the normalised Sulforhodamine G concentrations 300 seconds after the start of the dye injection. In the cases without bubbles (Figure 3, top row), mixing occurs due to the jet of the dye inlet and due to the counter-current liquid flow. In the stagnant case, the dye accumulates above the inlet, and large-scale, undisturbed dye structures can be found in the column, which is far from perfect mixing. Comparing this case to the cases with counter-current liquid flows, it becomes evident that with increasing counter-current liquid flow rate, the introduced dye heads towards the lower column regions and outlet at the bottom. The dye accumulation over the inlet is also decreased by the increased counter-current liquid flow rate, and the dye is transported downwards in high concentrated pockets.

In the presence of bubbles (Figure 3, bottom row), the large-scale structures vanish due to the bubble-generated upward flow and mixing is strongly enhanced. In the case without counter-current liquid flow and at the lowest counter-current flow rate, the injected dye is almost equally distributed in the whole measurement plane, except the inlet region, where the concentrated dye with higher intensities can be observed. With increasing counter-current flow rate, the low concentration region above the dye inlet spreads downward. At 55.5 l· min^{-1} counter-current liquid flow rate, the dye concentration is low (black regions) in the complete upper half of the column because the injected dye is completely transported downwards.

Copyright© Department of Fluid Mechanics, Budapest University of Technology and Economics and the Authors

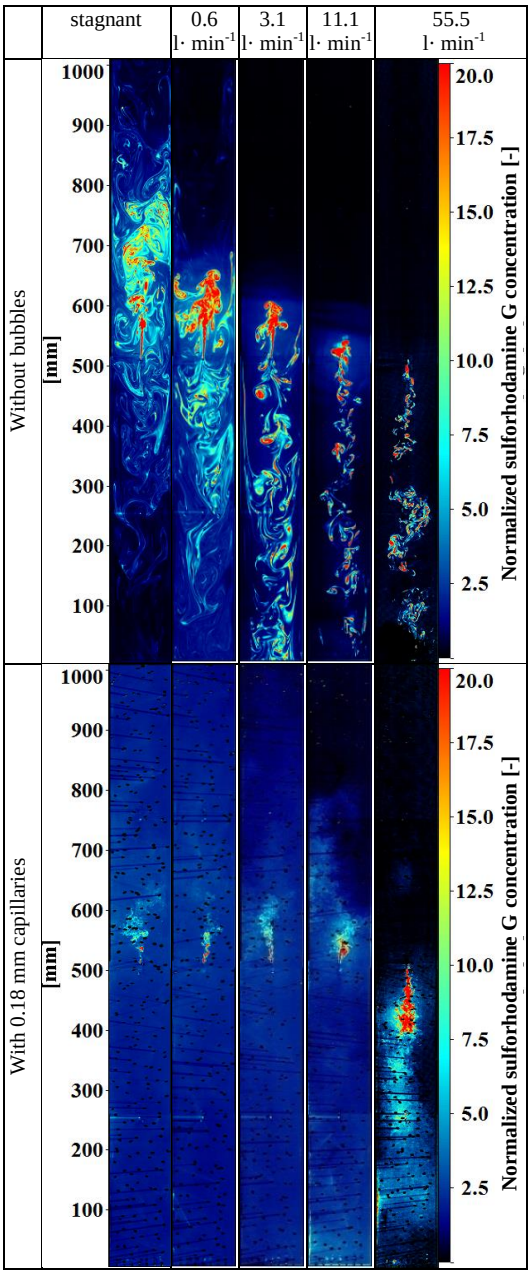

Figure 3. Snapshots of the experiments at t=300 s without (top) and with (bottom) bubbles. Dye inlet at 500 mm, bubbles generated with 0.18 capillaries at 10 l· h^{-1} gas flow rate.

Figure 4 compares the normalised concentration distributions over the column height for the investigated different inlet conditions. On these plots, conspicuous high peak concentrations can be recognised around the dye inlet at 55.5 l· min^{-1} counter-current liquid flow rate. As it was discussed before, the high counter-current liquid flow forces the dye to head downwards, and mixing is poor. Above the inlet, the dye concentration is close to zero in that case.

The stagnant and the two lowest counter-current liquid flow rates perform similar: except in the inlet region, the normalised concentration curves are rather equalised at values between one and two. In all these cases, the mixing efficiency increases with increasing counter-current liquid flow rate in the top half of the column.

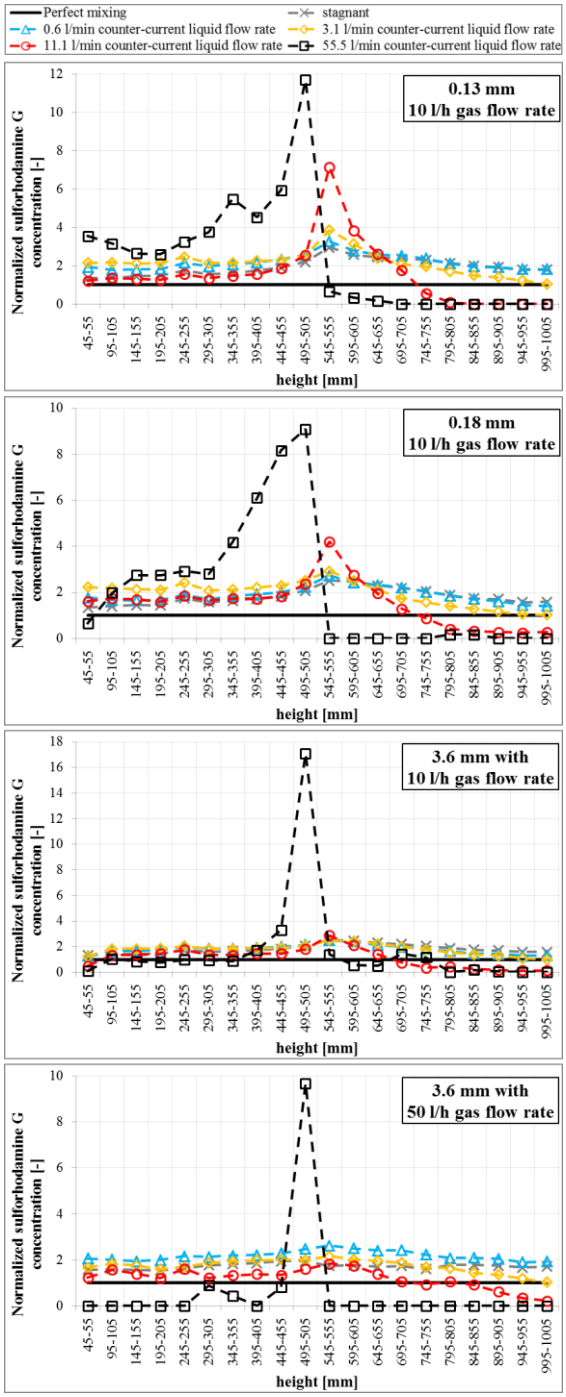

Figure 4. Normalized dye concentration ratios at t=300 s for different counter-current liquid flow rates in function of the column height. Dye inlet at 500 mm, bubbles generated with 0.13, 0.18 and 3.6 mm capillaries at 10 l· h^{-1} and 50 l· h^{-1} gas flow rates.

Copyright© Department of Fluid Mechanics, Budapest University of Technology and Economics and the Authors

In the case with the 3.6 mm capillary and 50 $l \cdot h^{-1}$ gas flow rate, this effect is visible over the complete column height. However, in all of the above-mentioned cases, the normalised values lay above perfect mixing. This means that the bubble-generated upward flow is strong enough to transport the dye to the upper half of the column, but mixing is not strong enough to distribute the dye homogeneously in the whole column. In the cases with 11.1 $l \cdot min^{-1}$ counter-current flow rate, a concentration peak also appears at the dye inlet, where the counter-current liquid flow forces the dye to head downwards. But, contrary to the lower counter-current liquid flow rates, just a small amount of dye is transported to the upper half of the column. Here, the bubble-generated upward liquid flow is definitely too weak to transport the dye to the top column section. However, with an increased gas flow rate, at 50 $l \cdot h^{-1}$, the dye concentration gets closer to perfect mixing also in the upper section, due to the stronger upward liquid flow. The best mixing performance has been found with the 3.6 mm capillary at 11.1 $l \cdot min^{-1}$ counter-current liquid and 50 $l \cdot h^{-1}$ gas flow rates, if the inlet is situated at 500 mm, in the middle of the column.

The analysis of the LIF results shows that a large difference exists between the mixing in cases with and without bubbles, but this difference gets less for all the cases with bubbles. For this reason, the vorticity of the liquid flow in the column was investigated, obtained from previous PIV measurements [32]. Vorticity is supposed to have an influence on mixing, since it is supported by the bubble-generated turbulence.

4.2. Bubble-generated turbulence

Figure 5 represents normalised Probability Density Functions (PDF) of the vorticity calculated from the PIV vector fields for the different investigated cases. The top plot shows the PDFs in the counter-current liquid flows, without bubbles. It was expected that with increasing counter-current liquid flow rate, and therefore with increasing Reynolds number from 100 to 9000, the vorticity increases and thus the PDFs get wider. When bubbles are in the flow, they disturb the existing flow pattern and generate additional turbulence. In Figure 5, these cases are shown in the bottom four plots for different capillary diameters, counter-current liquid and gas flow rates. The widths of the PDFs for the two small capillary diameters are comparable to the fully turbulent case (Re=9000, black squares) of the single-phase measurements in the top plot. It has also been found that in the presence of smaller bubbles, generated with the 0.13 and 0.18 mm capillaries, the vorticity distribution is independent of the counter-current liquid flow rate. Since the relative bubble velocity is the same for one given capillary diameter at all counter-current liquid flow rates, this result was expected.

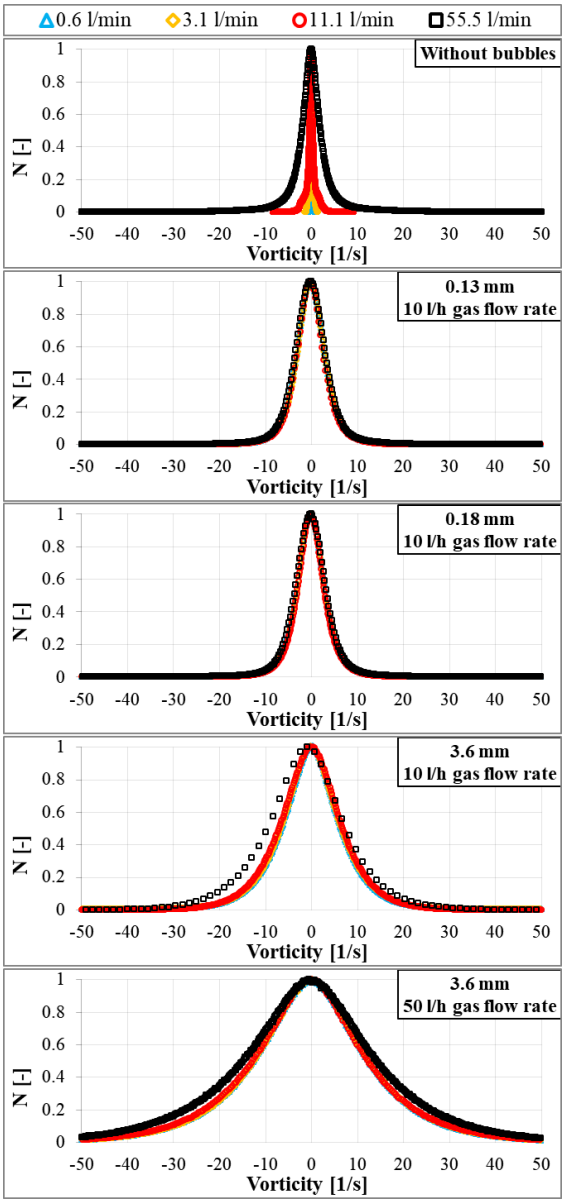

Figure 5. Normalized probability density functions of the vorticity for all investigated cases.

Interestingly, the vorticity distributions for these two inlet sizes are also very similar; however, there is a noticeable difference in bubble sizes as well as in aspect ratios (see in Table 2), and therefore in bubble velocities. This result explains the LIF mixing results on Figure 4, where also very similar dye distributions have been found for these two setups.

In the case of the larger bubbles, produced with the 3.6 mm capillaries, the vorticity distributions get even wider. This effect is further increased with increasing gas flow rate. In these cases, the mean bubble size is almost twice that of the smaller

Copyright© Department of Fluid Mechanics, Budapest University of Technology and Economics and the Authors

capillaries. These considerably larger bubbles generate larger and stronger vortex structures, which are reflected in the wider vorticity distributions. On these plots, the curve for 55.5 $l \cdot min^{-1}$ counter-current flow rate clearly separates from the others, while this was not observable on the distributions with smaller capillaries. The reason for that could be the size of the generated vortex structures. At 55.5 $l \cdot min^{-1}$ counter-current flow rate, the vorticity and the vortex structure sizes without bubbles are almost the same as in the cases with the 0.13 and 0.18 mm capillaries bubbles. Therefore, the vorticity distribution for this liquid flow rate remains almost the same with and without bubbles. Contrary to this, the larger bubbles produced with the 3.6 mm capillaries generate larger vortex structures, while the smaller structures from the initially turbulent liquid flow also remain.

The widest vorticity distribution has been found at the largest capillaries and the largest gas flow rate. This explains the mixing results, where the best mixing was also achieved with this setup.

5. CONCLUSIONS

In this paper bubble-induced mixing in a laboratory-scale bubble column has been investigated with LIF measurement technique, applying Sulforhodamine G as tracer dye, combined with shadow imaging. To support the analysis, the results of previous PIV experiments have also been examined. Capillaries with three different diameters were used to generate bubbles in a wide diameter range of 1 to 9 mm. The gas and liquid flow rates have been varied in this study as well.

It has been found that the presence of the bubbles, their size, the gas flow rate and the counter-current liquid flow rate have strong influences on mixing. The results have shown that the larger bubbles induce larger vortex structures, which leads to better mixing. Interestingly, no differences have been found in the vortex distributions between the cases with the two smaller capillaries, despite the noticeable differences in bubble size and aspect ratios.

The highest counter-current liquid flow rate led to a more concentrated dye jet, which was less dispersed than at lower liquid flow rates. The combination of large bubbles generated with the 3.6 mm capillaries and a moderate counter-current liquid flow rate 11.1 $l \cdot min^{-1}$, led to the best mixing performance in the bubble column.

ACKNOWLEDGEMENTS

This work has been carried out in the frame of a joint research project (GZ: RZ 11/3-1 and ZA 527/3-1) funded by the German Research Foundation (DFG). Instrumentation was funded by the Deutsche Forschungsgemeinschaft (DFG, German Research Foundation) – 279416000.

The authors would also like to acknowledge the help of their students Jianye Han, Maximilian Mahler and Steffen Erichson in doing the experiments and parts of the postprocessing. The workshop of LSS is acknowledged for its help in mounting the experimental set-up.

REFERENCES

[1] M. Ravinath, G. R. Kasat, A. B. Pandit, 2008, "Mixing Time in a Short Bubble Column", *The Canadian Journal of Chemical Engineering*, 2008, Vol. 81 (2), pp. 185-195. DOI: 10.1002/cjce.5450810203

[2] Z. Trad, J.-P. Fontaine, C. Larroche, C. Vial, 2017, "Experimental and numerical investigation of hydrodynamics and mixing in a dual-impeller mechanically-stirred digester", *Chem. Eng. J.*, 2017, Vol. 329, pp. 142-155. DOI: 10.1016/j.cej.2017.07.038

[3] F. Wang, N. D. Jin, D. Y. Wang, Y. F. Han, D. Y. Liu, 2017, "Measurement of gas phase characteristics in bubbly oil-gas-water flows using bi-optical fiber and high-resolution conductance probes", *Exp. Therm Fluid Sci.*, 2017, Vol. 88, pp. 361-375. DOI: 10.1016/j.expthermflusci.2017.06.017

[4] J.-L. Muñoz-Cobo, Y. Rivera, C. Berna, A. Escrivá, 2020, "Analysis of Conductance Probes for Two-Phase Flow and Holdup Applications", *Sensors*, 2020, Vol. 20 (24), pp. 7042. DOI: 10.3390/s20247042

[5] S. C. Low, N. Eshtiaghi, L. Shu, R. Parthasarathy, 2017, "Flow patterns in the mixing of sludge simulant with jet recirculation system", *Process Saf. Environ. Prot.*, 2017, Vol. 112, pp. 209-221. DOI: 10.1016/j.psep.2017.08.016

[6] L. A. Melton, C. W. Lipp, R. W. Spradling, K. A. Paulson, 2010, "Dismt - Determination of mixing time through color changes", *Chem. Eng. Commun.*, 2010, Vol. 189 (3), pp. 322-338. DOI: 10.1080/00986440212077

[7] S. A. Hashemi, R. B. Spelay, R. S. Sanders, B. T. Hjertaker, 2021, "A novel method to improve Electrical Resistance Tomography measurements on slurries containing clays", *Flow Measurement and Instrumentation*, 2021, Vol. 80, pp. 101973. DOI: 10.1016/j.flowmeasinst.2021.101973

[8] S. C. Low, D. Allitt, N. Eshtiaghi, R. Parthasarathy, 2018, "Measuring active volume using electrical resistance tomography in a gas-sparged model anaerobic digester", *Chem. Eng. Res. Des.*, 2018, Vol. 130, pp. 42-51. DOI: 10.1016/j.cherd.2017.11.039

[9] J. Coppeta, C. Rogers, 1998, "Dual emission laser induced fluorescence for direct planar scalar behavior measurements", *Exp.*

Copyright© Department of Fluid Mechanics, Budapest University of Technology and Economics and the Authors

Fluids, 1998, Vol. 25 (1), pp. 1-15. DOI: 10.1007/s003480050202

[10] X. Wang, R. Wang, S. Du, J. Chen, S. Tan, 2016, "Flow visualization and mixing quantification in a rod bundle using laser induced fluorescence", *Nucl. Eng. Des.*, 2016, Vol. 305, pp. 1-8. DOI: 10.1016/j.nucengdes.2016.01.007

[11] A. Eltayeb, S. Tan, Z. Qi, A. A. Ala, N. M. Ahmed, 2019, "PLIF experimental validation of a FLUENT CFD model of a coolant mixing in reactor vessel down-comer", *Ann. Nucl. Energy*, 2019, Vol. 128, pp. 190-202. DOI: 10.1016/j.anucene.2018.12.051

[12] G. Montante, A. Paglianti, 2015, "Fluid dynamics characterization of a stirred model bio-methanation digester", *Chem. Eng. Res. Des.*, 2015, Vol. 93, pp. 38-47. DOI: 10.1016/j.cherd.2014.05.003

[13] E. Bouche, S. Cazin, V. Roig, F. Risso, 2013, "Mixing in a swarm of bubbles rising in a confined cell measured by mean of PLIF with two different dyes", *Exp. Fluids*, 2013, Vol. 54 (6), pp. DOI: 10.1007/s00348-013-1552-0

[14] E. Alméras, S. Cazin, V. Roig, F. Risso, F. Augier, C. Plais, 2016, "Time-resolved measurement of concentration fluctuations in a confined bubbly flow by LIF", *Int. J. Multiphase Flow*, 2016, Vol. 83, pp. 153-161. DOI: 10.1016/j.ijmultiphaseflow.2016.03.011

[15] E. Alméras, C. Plais, V. Roig, F. Risso, F. Augier, 2018, "Mixing mechanisms in a low-sheared inhomogeneous bubble column", *Chem. Eng. Sci.*, 2018, Vol. 186, pp. 52-61. DOI: https://doi.org/10.1016/j.ces.2018.04.026

[16] T. Ma, H. Hessenkemper, D. Lucas, A. D. Bragg, 2022, "An experimental study on the multiscale properties of turbulence in bubble-laden flows", *J. Fluid Mech.*, 2022, Vol. 936, pp. DOI: 10.1017/jfm.2022.86

[17] T. Ma, H. Hessenkemper, D. Lucas, A. D. Bragg, 2023, "Effects of surfactants on bubble-induced turbulence", *J. Fluid Mech.*, 2023, Vol. 970, pp. DOI: 10.1017/jfm.2023.614

[18] T. Ma, B. Ott, J. Fröhlich, A. D. Bragg, 2021, "Scale-dependent anisotropy, energy transfer and intermittency in bubble-laden turbulent flows", *J. Fluid Mech.*, 2021, Vol. 927, pp. DOI: 10.1017/jfm.2021.760

[19] T. Ma, C. Santarelli, T. Ziegenhein, D. Lucas, J. Fröhlich, 2017, "Direct numerical simulation–based Reynolds-averaged closure for bubble-induced turbulence", *Physical Review Fluids*, 2017, Vol. 2 (3), pp. DOI: 10.1103/PhysRevFluids.2.034301

[20] D. Wiemann, D. Mewes, 2005, "Prediction of Backmixing and Mass Transfer in Bubble Columns Using a Multifluid Model", *Industrial & Engineering Chemistry Research*, 2005, Vol. 44 (14), pp. 4959-4967. DOI: 10.1021/ie049163c

[21] W. Bai, N. G. Deen, J. A. M. Kuipers, 2011, "Numerical Investigation of Gas Holdup and Phase Mixing in Bubble Column Reactors", *Industrial & Engineering Chemistry Research*, 2011, Vol. 51 (4), pp. 1949-1961. DOI: 10.1021/ie102557h

[22] K. Ekambara, J. B. Joshi, 2008, "CFD Simulation of Residence Time Distribution and Mixing in Bubble Column Reactors", *The Canadian Journal of Chemical Engineering*, 2008, Vol. 81 (3-4), pp. 669-676. DOI: 10.1002/cjce.5450810345

[23] D. Bothe, H. Shirzadi, H. J. Warnecke, 2007, "Evaluations of Euler–Euler Simulations of Bubble Columns Based on Numerical Tracer Experiments", *Chem. Eng. Res. Des.*, 2007, Vol. 85 (11), pp. 1491-1496. DOI: 10.1205/cherd06249

[24] Y. Jin, R. F. Cavero, C. Weiland, M. Hoffmann, M. Schlüter, 2023, "Effects of bubble-induced turbulence on interfacial species transport: A direct numerical simulation study", *Chem. Eng. Sci.*, 2023, Vol. 279, pp. 118934. DOI: 10.1016/j.ces.2023.118934

[25] J. B. Joshi, K. Nandakumar, G. M. Evans, V. K. Pareek, M. M. Gumulya, M. J. Sathe, M. A. Khanwale, 2017, "Bubble generated turbulence and direct numerical simulations", *Chem. Eng. Sci.*, 2017, Vol. 157, pp. 26-75. DOI: https://doi.org/10.1016/j.ces.2016.03.041

[26] J. Liu, X. Guan, N. Yang, 2023, "Bubble-induced turbulence in CFD simulation of bubble columns. Part I: Coupling of SIT and BIT", *Chem. Eng. Sci.*, 2023, Vol. 270, pp. 118528. DOI: 10.1016/j.ces.2023.118528

[27] R. Rzehak, E. Krepper, 2013, "CFD modeling of bubble-induced turbulence", *Int. J. Multiphase Flow*, 2013, Vol. 55, pp. 138-155. DOI: 10.1016/j.ijmultiphaseflow.2013.04.007

[28] R. Zamansky, F. Le Roy De Bonneville, F. Risso, 2024, "Turbulence induced by a swarm of rising bubbles from coarse-grained simulations", *J. Fluid Mech.*, 2024, Vol. 984, pp. DOI: 10.1017/jfm.2024.230

[29] P. Kováts, K. Zähringer, Year, "Bubble induced mixing in a bubble column with counter-current liquid flow", Proc. *21st International Symposium on the Application of Laser and Imaging Techniques to Fluid Mechanics*, Lisbon, Portugal, pp. 23/1-19.

[30] H. Khan, P. Kováts, K. Zähringer, R. Rzehak, 2024, "Experimental and numerical investigation of a counter-current flow bubble column", *Chem. Eng. Sci.*, 2024, Vol.

Copyright© Department of Fluid Mechanics, Budapest University of Technology and Economics and the Authors

285, pp. 119503. DOI: 10.1016/j.ces.2023.119503
[31] P. Kováts, 2021, "Detailed experimental study of mass transfer and liquid flow in a bubble column with optical measurement techniques", *PhD*, Otto-von-Guericke-Universität Magdeburg (Magdeburg).
[32] P. Kováts, K. Zähringer, 2024, "Statistical Analysis of Bubble Parameters from a Model Bubble Column with and without Counter-Current Flow", *Fluids*, 2024, Vol. 9 (6), pp. 126. DOI: 10.3390/fluids9060126

Copyright© Department of Fluid Mechanics, Budapest University of Technology and Economics and the Authors